Journal of Biomechanics 45 (2012) 2743–2749

Contents lists available at SciVerse ScienceDirect

Journal of Biomechanics

journal homepage: www.elsevier.com/locate/jbiomech
www.JBiomech.com

# The relative influence of apatite crystal orientations and intracortical porosity on the elastic anisotropy of human cortical bone

Andrew P. Baumann, Justin M. Deuerling, David J. Rudy, Glen L. Niebur, Ryan K. Roeder *

*Department of Aerospace and Mechanical Engineering, University of Notre Dame, Notre Dame, IN 46556, USA*

ARTICLE INFO

*Article history:*
Accepted 6 September 2012

*Keywords:*
Cortical bone
Elastic anisotropy
Finite element model
Micromechanical model
Micro-computed tomography
Haversian porosity
Intracortical porosity
Orientation distribution function

ABSTRACT

Elastic anisotropy exhibits spatial inhomogeneity in human cortical bone, but the structural origins of anatomic variation are not well understood. In this study, the elastic anisotropy of human cortical bone was predicted using a specimen-specific multiscale model that investigated the relative influence of apatite crystal orientations and intracortical porosity. The elastic anisotropy of cortical bone specimens from the diaphysis of human femora was measured by ultrasonic wave propagation as the ratio of elastic constants in the longitudinal/radial ($L/R$) and longitudinal/circumferential ($L/C$) anatomic specimen axes. Experimental measurements of elastic constants exhibited orthotropy, with greater anisotropy in the $L/R$ plane compared to the $L/C$ plane. Model predictions included (1) a micromechanical model accounting for the effects of apatite crystal orientations, (2) a voxel-based finite element model accounting for the effects of intracortical porosity, and (3) a combined model accounting for both effects. The combined model provided the most accurate predictions of elastic anisotropy in both the $L/R$ and $L/C$ plane, with less than 10% mean error. The micromechanical model alone was able to accurately predict elastic anisotropy in the $L/C$ plane, but predicted transverse isotropy. The finite element model alone grossly underestimated elastic anisotropy in both the $L/R$ and $L/C$ planes, but was able to predict orthotropy. Therefore, the results of this study suggest that the dominant and less variable transverse isotropy of human cortical bone, reflected by $L/C$, is governed primarily by apatite crystal orientations, while the more subtle and variable orthotropy, reflected by the difference between $L/R$ and $L/C$, is governed primarily by intracortical porosity. Moreover, the combined model may be useful to investigate other structure-function relationships or in place of current numerical models, for example, in the study of bone adaptation and metabolic bone disease.



## 1. Introduction

The elastic properties of human cortical bone are orthotropic, with the elastic constant in the longitudinal ($L$) bone axis being the greatest, followed by the circumferential ($C$) and radial ($R$) axes (Ashman et al., 1984; Espinoza Orías et al., 2009; Rudy et al., 2011). The elastic anisotropy of human cortical bone is essential to its load-bearing function as elastic constants are greatest in the longitudinal bone axis. Elastic anisotropy also exhibits spatial inhomogeneity in cortical bone, varying with anatomic location (Espinoza Orías et al., 2009; Rudy et al., 2011). However, few studies have attempted to predict variability in elastic anisotropy (Deuerling et al., 2009) such that it could be incorporated in numerical models of cortical bone in a manner similar to accounting for elastic inhomogeneity using power-law scaling relationships (Hernandez et al., 2001; Keller et al., 1990; Schaffler and Burr, 1988; Zioupos et al., 2008).

Elastic anisotropy in cortical bone has been attributed to a number of microstructural features, such as intracortical porosity (Currey and Zioupos, 2001; Dong and Guo, 2004; Mullins et al., 2007; Sansalone et al., 2010; Sevostianov and Kachanov, 2000) and osteons (Aoubiza et al., 1996; Dong and Guo, 2006; Hogan, 1992; Katz, 1980), as well as the organization of the constituent materials, apatite crystals (Akkus, 2005; Currey, 1969; Deuerling et al., 2009; Hasegawa et al., 1994; Turner et al., 1995; Wagner and Weiner, 1992) and collagen molecules (Hellmich and Ulm, 2002; Lees and Davidson, 1977). Thus, the elastic anisotropy observed at the tissue level is due to the concomitant effects of these structural parameters combined across multiple length scales (Deuerling et al., 2009; Hamed et al., 2010). The relative influence of individual structural features is often difficult to investigate experimentally, but can be decoupled using analytical and computational models.

A specimen-specific multiscale micromechanical model was able to accurately predict the elastic anisotropy of human cortical bone specimens by accounting for the orientation distribution of

* Correspondence to: Associate Professor, Department of Aerospace and Mechanical Engineering, Bioengineering Graduate Program, 148 Multidisciplinary Research Building, University of Notre Dame, Notre Dame, IN 46556.
Tel.: +1 574 631 7003; fax: +1 574 631 2144.
*E-mail address:* rroeder@nd.edu (R.K. Roeder).

0021-9290/$ - see front matter © 2012 Elsevier Ltd. All rights reserved.
http://dx.doi.org/10.1016/j.jbiomech.2012.09.011

apatite crystals among six other structural parameters (Deuerling et al., 2009). Structural parameters included the apatite crystal orientation distribution function (ODF), volume fraction, aspect ratio, and elastic constants; the collagen elastic constants; and the Haversian porosity volume fraction and aspect ratio. This micromechanical model can be modified to remove the contribution of intracortical porosity, facilitating elastic anisotropy predictions accounting for the effects of apatite crystal orientations alone.

Micro-finite element models have been used to investigate the effects of tissue porosity on the elastic inhomogeneity and anisotropy of both cortical bone (Burghardt et al., 2010) and trabecular bone (Niebur et al., 2000; van Rietbergen et al., 1996; van Rietbergen et al., 1998). Three-dimensional micro-computed tomography (micro-CT) reconstructions of tissues may be obtained with sufficient resolution to segment the tissue porosity, including Haversian canals and resorption cavities, so that bone voxels can be converted to hexahedral elements. Therefore, these voxel-based finite element models are able to precisely account for the volume fraction, morphology, orientation, and spatial distribution of intracortical porosity, facilitating elastic anisotropy predictions accounting for the effects of intracortical porosity alone.

The aims of this study were to predict the elastic anisotropy of human cortical bone using a specimen-specific multiscale model that investigated the relative influence of apatite crystal orientations and intracortical porosity. The elastic anisotropy was measured by ultrasonic wave propagation and then predicted using a micromechanical model accounting for the effects of apatite crystal orientations, a voxel-based finite element model accounting for the effects of intracortical porosity, and a combined model accounting for both effects.

## 2. Materials and methods

### 2.1. Human cortical bone specimens

A total of 48 parallelepiped cortical bone specimens, nominally $5\times5\times2-5$ mm, were prepared from the femoral diaphyses of two male (ages 18 and 53) and two female (ages 41 and 59) human donors which were received as fresh frozen tissue. All donors presented no toxicology or bone-related pathology. All tissues were obtained with donor's consent (National Disease Research Interchange, Philadelphia, PA) and all protocols were approved by the Notre Dame Human Subjects Institutional Review Board. Samples were taken from each of the four anatomic quadrants (anterior, medial, posterior, lateral) at three locations along the length of the diaphysis (20%, 50%, and 80% of total femoral length) for a total of 12 specimens per donor (Fig. 1). Two specimens were omitted from the study due to exhibiting porosity that exceeded 30%, which was taken as an upper limit for cortical bone (Zioupos et al., 2008). Cortical bone specimens were stored at $-20$ °C in a solution of 50% ethanol and 50% phosphate buffered saline during interim periods, and returned to a fully hydrated state prior to mechanical characterization. An orthogonal curvilinear coordinate system with radial ($R$), circumferential ($C$), and longitudinal ($L$) axes was defined by the anatomic shape of the femoral diaphysis (Fig. 1).

### 2.2. Elastic constants

Longitudinal elastic constants were measured for each specimen in each of the three orthogonal directions ($C_L$, $C_C$, and $C_R$) using the pulse-transmission method for ultrasonic wave propagation, as described in detail elsewhere (Espinoza Orías et al., 2009; Rudy et al., 2011). Elastic anisotropy was measured as the ratio of longitudinal elastic constants in the $L/R$ ($C_L/C_R$) and $L/C$ ($C_L/C_C$) specimen planes. The elastic anisotropy ratio in the $R/C$ specimen plane was dependent on the other two ratios and was therefore not considered.

### 2.3. Micromechanical model

The contribution of apatite crystal orientations to the elastic anisotropy of cortical bone tissue was evaluated using a micromechanical model accounting for the volume fraction, aspect ratio and orientation of the apatite crystals within the extracellular matrix (ECM). In contrast to previous use of the model (Deuerling et al., 2009), the effects of intracortical porosity were not considered. Therefore, micromechanical model predictions accounted for the effects of apatite crystal orientations alone (Fig. 1).

At the first level of the model, the elastic constants of a mineralized collagen fibril were modeled using the Halpin–Tsai equations for a representative volume element (RVE) comprising perfectly aligned apatite crystals as discontinuous square fiber reinforcements within a continuous isotropic collagen matrix (Halpin, 1992). The Halpin–Tsai equations accounted for the elastic constants and volume fractions of the constituent phases, as well as the aspect ratio of the apatite crystals (Table 1). At the second level of the model, the effective elastic constants of the ECM were calculated by averaging the weighted contribution of all misoriented RVEs by the experimentally measured ODF as

$$\overline{C}_{\mathrm{ECM}}=\frac{\int C_{\mathrm{RVE}}(\theta)\cdot g(\theta)\cdot d\theta}{\int g(\theta)\cdot d\theta} \quad (1)$$

where $\theta$ is the angle of misorientation between the longitudinal specimen axis and the elongated $c$-axis of apatite crystals, $g(\theta)$ is the ODF, and $C_{\mathrm{RVE}}(\theta)$ is the stiffness tensor calculated for the misoriented RVE in the sample coordinate system after tensor transformation by $\theta$ (Deuerling et al., 2009; Yue and Roeder, 2006).

The apatite crystal ODF was measured for each specimen by quantitative texture analysis using an X-ray diffractometer equipped with an area detector (D8 Discover with GADDS, HI-STAR, Bruker AXS, Madison, WI) using methods previously established (Deuerling et al., 2009; Deuerling et al., 2012). Specimens were mounted on a goniometer that allowed for accurate six-axis positioning of the polished longitudinal specimen face. Pole figures were measured for three crystallographic planes (222, 213 and 004), and data was normalized by randomly oriented samples prepared from deproteinized and ground cortical bone tissue. ODFs were calculated from the normalized pole figures by the Arbitrarily Defined Cells (ADC) method (LaboTex 2.1, LaboSoft s.c., Poland). Two-dimensional (2-D) ODFs for the misorientation of apatite crystals in the $L/R$ and $L/C$ planes were obtained from the measured three-dimensional (3-D) ODF, such that micromechanical model predictions for $C_L$ and $C_R$ used the $L/R$ plane ODF and predictions for $C_L$ and $C_C$ used the $L/C$ plane ODF (Deuerling et al., 2012). Elastic anisotropy was quantified by the ratio of elastic constants in the $L/R$ and $L/C$ specimen planes. Note that measured 3-D ODFs were typically axisymmetric which resulted in the prediction of transversely isotropic elastic constants ($C_C\approx C_R$) and no difference in the elastic anisotropy ratios ($L/C\approx L/R$), but transverse isotropy was not assumed *a priori* in the micromechanical model.

### 2.4. Finite element model

The contribution of intracortical porosity to the elastic anisotropy was evaluated using voxel-based finite element models accounting for the volume

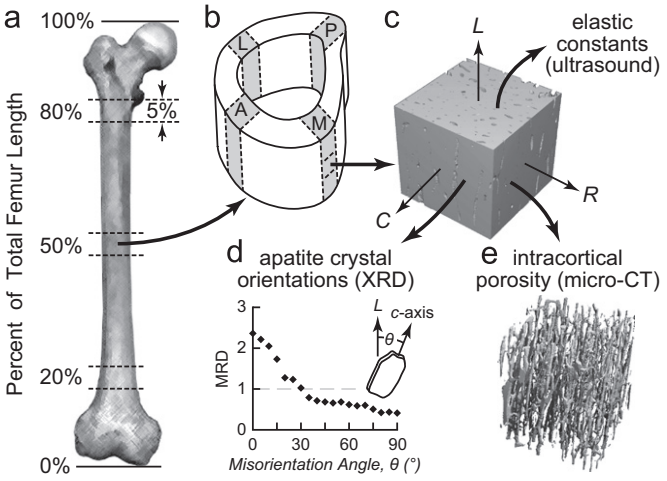


**Fig. 1.** Cortical bone specimens were prepared from (a) the diaphysis of whole human femora at 20, 50, and 80% of total femoral length in (b) each anatomic quadrant ($A$=anterior, $M$=medial, $P$=posterior, and $L$=lateral) using (c) an orthogonal curvilinear coordinate system ($L$=longitudinal, $C$=circumferential, and $R$=radial). Longitudinal elastic constants in each specimen axis were measured experimentally using ultrasonic wave propagation. The micromechanical model accounted for the effect of apatite crystal orientations on the elastic anisotropy using specimen-specific measurements of the apatite crystal orientation distribution (ODF) function from X-ray diffraction. (d) A representative 2-D ODF shows the relative probability in multiples of a random distribution (MRD, where a value of one corresponds to a random distribution) for a volume of crystals having a given misorientation angle ($\theta$) between the specimen axis and apatite crystal $c$-axis. (e) The finite element model accounted for the effects of intracortical porosity on the elastic anisotropy using voxel-based models created from segmented micro-CT images.

**Table 1**
Structural parameters used for the micromechanical model accounting for the effects of apatite crystals on the elastic anisotropy.

| Phase | Parameter | Value(s) | Reference |
|---|---|---|---|
| Apatite crystals | Elastic constants (transversely isotropic) | $C_{11}$=137 GPa<br>$C_{33}$=172 GPa<br>$C_{12}$=42.5 GPa<br>$C_{13}$=54.9 GPa<br>$C_{44}$=39.6 GPa | Katz and Ukraincik (1971) |
| | ODF | *measured* | |
| | Volume fraction | ~0.5 | Fratzl et al. (1996) |
| | Mean aspect ratio | ~20 | Eppell et al. (2001) |
| Collagen | Elastic constants (isotropic) | $C_{11}$=3.9 GPa<br>$C_{12}$=1.1 GPa | Sasaki and Odajima (1996) |
| | Volume fraction | ~0.5 | Fratzl et al. (1996) |

fraction, morphology, orientation, and spatial distribution of intracortical porosity. All specimens were imaged by micro-CT (μCT-80, Scanco Medical AG, Brüttisellen, Switzerland) at 70 kVp, 114 μA and 400 ms integration time with a 10 μm isotropic voxel size, which was sufficient to resolve the Haversian canals and resorption cavities that comprise the intracortical porosity (Fig. 1). Images were segmented using a Gaussian filter (sigma=0.8, support=1) followed by a global threshold corresponding to a linear attenuation of 1.92 $cm^{-1}$, or 717 mg HA/$cm^3$ based on a custom hydroxyapatite (HA) calibration phantom (Deuerling et al., 2010). The overall mean (±standard deviation) intracortical porosity measured by micro-CT for the specimens was 8.1 (4.8) vol%.

Finite element models were generated for each specimen by directly converting the bone voxels to 8-node hexahedral elements. The models had between 6 and 90 million elements, yielding between 16 and 270 million degrees of freedom. An isotropic elastic modulus of 17 GPa and a Poisson's ratio of 0.3 was assumed for the ECM. Each model was solved for six pure strain conditions by applying displacements to all six faces of the specimen to induce uniform external strain, and the full $6\times6$ elastic constant tensor was determined from the calculated stresses in reference to the sample coordinate system (van Rietbergen et al., 1996). As before, the elastic anisotropy ratios in the $L/R$ ($C_L/C_R$) and $L/C$ ($C_L/C_C$) specimen planes were calculated. Since the ECM was assumed to be isotropic, finite element model predictions reflected the effects of intracortical porosity alone (Fig. 1). Computations were performed using a custom parallelized linear elastic finite element code on 96 processors utilizing 124 GB of memory. The average CPU time per model was approximately 72 h.

### 2.5. Combined model

A combined model was constructed to couple the effects of apatite crystal orientations and intracortical porosity using the above micromechanical and finite element models. The anisotropic elastic constants derived from the micromechanical model were assigned to the finite elements with material axes aligned with the three orthogonal axes of the bone specimens. In this manner, the ECM in the finite element model was assigned homogeneous, specimen-specific, anisotropic elastic constants. Therefore, combined model predictions of elastic anisotropy accounted for the effects of both intracortical porosity and apatite crystal orientations. The complete elastic constant tensor was again calculated from six uniaxial strain conditions, and the anisotropy ratios were calculated.

### 2.6. Statistical methods

Model predictions were compared with experimentally measured elastic anisotropy ratios using analysis of variance (ANOVA) (JMP 9.0.2, SAS Institute Inc., Cary, NC). *Post-hoc* comparisons were performed using Tukey's HSD test. The measured and predicted elastic symmetry was evaluated using paired $t$-tests to examine differences in the elastic anisotropy ratios for the $L/R$ versus $L/C$ planes. The correlation of model predictions with experimentally measured elastic anisotropy ratios was examined using linear least-squares regression. The level of significance for all tests was set at $p<0.05$.

## 3. Results

The elastic anisotropy of human cortical bone specimens as measured experimentally by ultrasonic wave propagation exhibited, at most, orthotropic symmetry with $L/R>L/C$ ($p<0.0001$, paired $t$-test) (Fig. 2, Table 2). The finite element model accounting for the effects of intracortical porosity alone significantly underestimated elastic anisotropy in both the $L/R$ and $L/C$ planes ($p<0.0001$, Tukey) (Fig. 2). However, the finite element model predicted orthotropy with $L/R>L/C$ ($p<0.0001$, paired $t$-test). The micromechanical model accounting for the effects of the apatite crystal orientations alone accurately predicted the $L/C$ anisotropy ratio ($p>0.90$, Tukey), but significantly underestimated the $L/R$ ratio ($p<0.0001$, Tukey) (Fig. 2). The micromechanical model predicted transverse isotropy with $L/R=L/C$ ($p=1.00$, paired $t$-test) (Table 2).

The combined model accounting for both effects provided the most accurate predictions of elastic anisotropy in both the $L/C$ ($p=0.11$, Tukey) and $L/R$ plane (Fig. 2). Although the anisotropy ratio in the $L/R$ plane was underestimated ($p<0.0001$, Tukey), the mean error was less than 10% and was the lowest of all three models (Table 3). The combined model also predicted orthotropy with $L/R>L/C$ ($p<0.0001$, paired $t$-test) (Table 2). Elastic anisotropy predictions for the combined model were correlated with experimental measurements in the $L/C$ plane ($p<0.01$), but not the $L/R$ plane ($p=0.35$) (Fig. 3). The lack of correlation in the $L/R$ plane appeared to be due to anatomic variability along the length of the femoral diaphysis that the model did not account for (Fig. 3a).

Experimentally measured elastic anisotropy ratios in the $L/R$ plane exhibited differences along the length of the femoral diaphysis, increasing from the mid-diaphysis to the epiphyses ($p<0.0001$, ANOVA) (Fig. 4a). However, all model predictions for elastic anisotropy in the $L/R$ plane exhibited no differences between locations along the femoral diaphysis ($p>0.38$, ANOVA). The elastic anisotropy ratio in the $L/C$ plane did not vary along the length of the femoral diaphysis for both experimental measurements ($p=0.29$, ANOVA) and model predictions ($p>0.17$, ANOVA) (Fig. 4b).

## 4. Discussion

The relative influence of apatite crystal orientations and intracortical porosity on the elastic anisotropy of human cortical bone tissue was decoupled using a micromechanical model and voxel-based finite element model, respectively, to separately account for each effect. The micromechanical model was able to accurately predict elastic anisotropy in the $L/C$ specimen plane (Fig. 2), but predicted transverse isotropy instead of orthotropy (Table 3). In contrast, the finite element model grossly underestimated elastic anisotropy in both the $L/R$ and $L/C$ planes (Fig. 2), but was able to predict orthotropy (Table 3). These results suggest that the dominant and less variable transverse isotropy of human cortical bone, reflected by $L/C$, is governed primarily by apatite crystal orientations, while the more subtle and variable orthotropy, reflected by the difference between $L/R$ and $L/C$, is governed primarily by intracortical porosity.

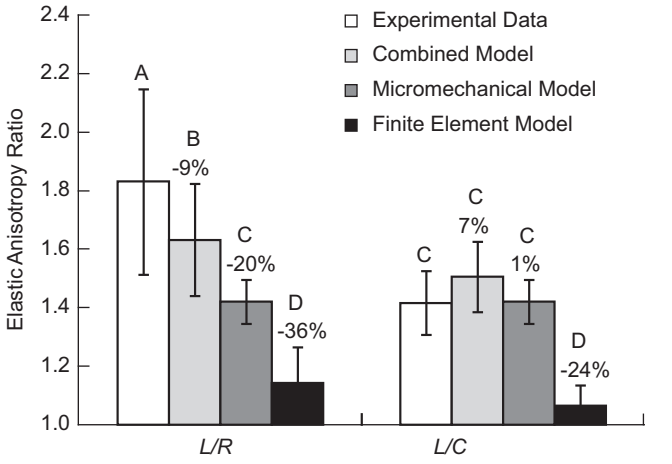


**Fig. 2.** Comparison of the mean (± standard deviation) elastic anisotropy ratios measured experimentally versus predictions by the finite element model accounting for the effects of intracortical porosity alone, the micromechanical model accounting for the effects of apatite crystal orientations alone, and the combined model accounting for both effects. Differences between values not connected by the same letter were statistically significant ($p < 0.05$, Tukey). The mean error (%) of model predictions is shown above each bar and in Table 3. Elastic symmetry was investigated by paired comparisons between anisotropy ratios in the *L*/*R* and *L*/*C* specimen planes as shown in Table 2.

**Table 2**
Overall mean (± standard deviation) elastic anisotropy ratios in the *L*/*R* and *L*/*C* specimen planes for experimental measurements and model predictions. Elastic symmetry was investigated by differences between *L*/*R* and *L*/*C* using paired *t*-tests.

| Method | Anisotropy ratio | | *p*-value |
|---|---|---|---|
| | *L*/*R* | *L*/*C* | |
| Experimental data | 1.83 (0.32) | 1.42 (0.11) | < 0.0001 |
| Micromechanical model | 1.42 (0.07) | 1.42 (0.07) | 1.00 |
| Finite element model | 1.14 (0.12) | 1.07 (0.07) | < 0.0001 |
| Combined model | 1.63 (0.19) | 1.51 (0.12) | < 0.0001 |

**Table 3**
Mean and mean absolute error (± standard deviation) between model predictions and experimental measurements for elastic anisotropy ratios in the *L*/*R* and *L*/*C* specimen planes.

| Model type | Mean error (%) | | Mean absolute error (%) | |
|---|---|---|---|---|
| | *L*/*C* | *L*/*R* | *L*/*C* | *L*/*R* |
| Micromechanical model | 0.7 (7.7) | −20.3 (13.9) | 6.1 (4.7) | 21.4 (12.1) |
| Finite element model | −24.4 (7.3) | −36.1 (11.3) | 24.4 (7.3) | 36.1 (11.3) |
| Combined model | 6.7 (9.6) | −8.7 (17.0) | 9.1 (7.3) | 15.6 (10.8) |

The overall degree of elastic anisotropy in human cortical bone tissue was primarily due to the preferred orientation of apatite crystals (Fig. 2). A parametric study using a previous specimen-specific micromechanical model that accounted for seven structural parameters across multiple length scales also identified the apatite crystal orientation distribution to be the most significant structural parameter governing the elastic anisotropy of cortical bone (Deuerling et al., 2009). However, micromechanical model predictions accounting for the effects of apatite crystal orientations alone, underestimated the magnitude and variability of elastic anisotropy in the *L*/*R* plane (Figs. 2 and 3), which was not surprising since specimen-specific measurements of the 3-D ODF for apatite crystals were axisymmetric. Therefore, although most elastic anisotropy at the tissue level is derived from the

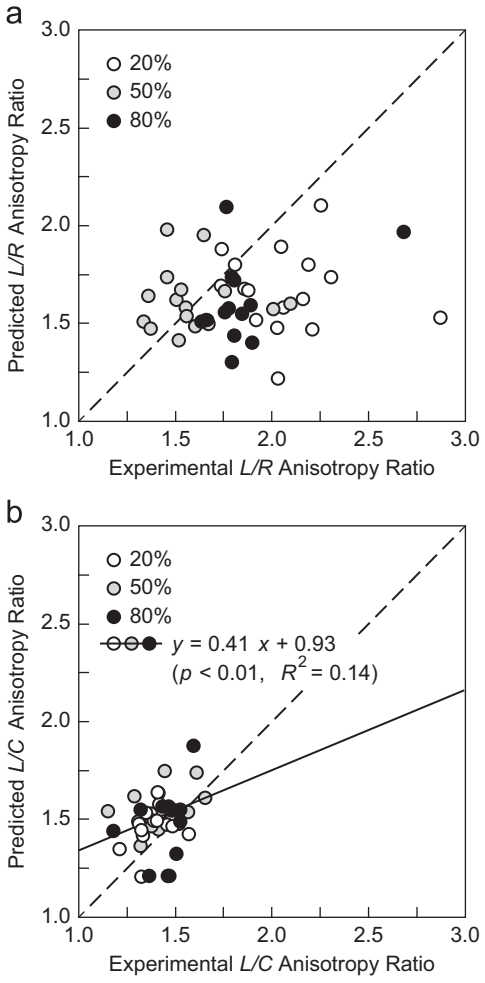


**Fig. 3.** Elastic anisotropy predictions by the combined model accounting for both apatite crystal orientations and intracortical porosity were not correlated with experimental measurements in the (a) *L*/*R* specimen plane, but were correlated with experimental measurements in the (b) *L*/*C* specimen plane, using least squares regression. Data points show specimens taken from 20, 50, and 80% of the total femoral length, which were pooled for regression analyses.

preferred orientation of apatite crystals, other factors must account for the greater magnitude and variability of elastic anisotropy in the *L*/*R* plane compared to the *L*/*C* plane.

The orthotropy ($L/R > L/C$) and variability of elastic anisotropy in the *L*/*R* plane was primarily due to the effects of intracortical porosity in human cortical bone tissue (Fig. 2). Another recent study also concluded that intracortical porosity was the major determinant of variability in the magnitude of elastic constants in cortical bone (Granke et al., 2011). However, this study did not consider orthotropy due to sampling tissue exclusively from the femoral mid-diaphysis and assumed an idealized pore architecture. In contrast, the voxel-based finite element model in the present study included the specimen-specific effects of the volume fraction, morphology, orientation, and spatial distribution of intracortical porosity. These effects are well-known to vary with anatomic location (Bousson et al., 2001; Espinoza Orías et al., 2009; Thomas et al., 2005) and donor age or gender (Bousson et al., 2001; Cooper et al., 2007; Feik et al., 1997; Thomas et al., 2005; Zebaze et al., 2010). An increased volume fraction of intracortical porosity has been shown to decrease elastic constant magnitudes (Burghardt et al., 2010; Hernandez et al., 2001; Keller et al., 1990; Schaffler and Burr, 1988; Zioupos et al., 2008) and increase anisotropy (Deuerling et al., 2009; Espinoza Orías et al., 2009; Mullins et al., 2007; Sansalone et al., 2010; Sevostianov and

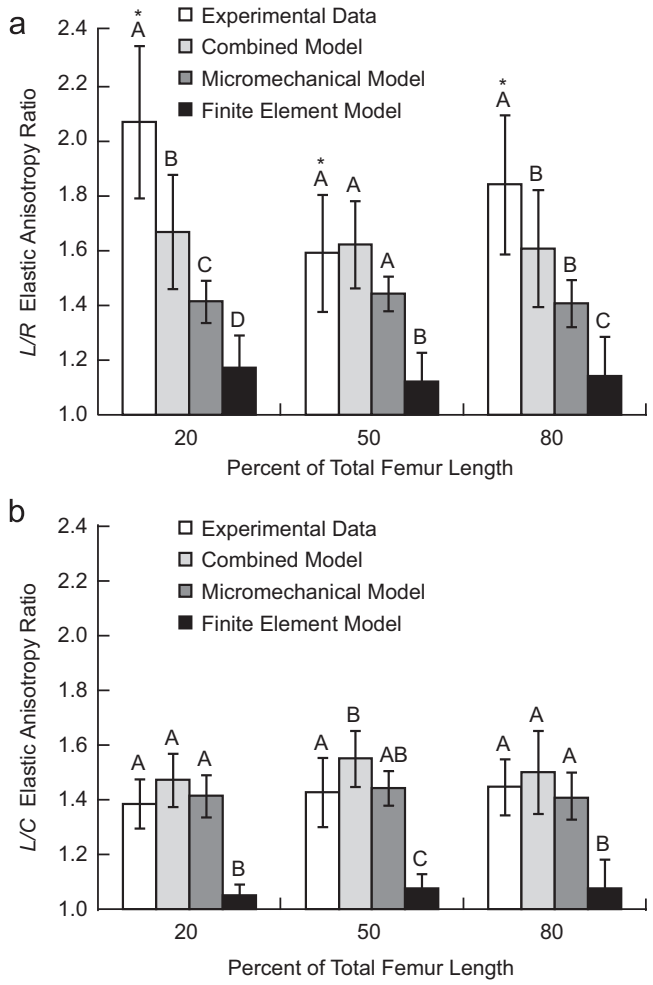


**Fig. 4.** Comparison of experimental measurements and model predictions for the mean ( ± standard deviation) elastic anisotropy ratio in the (a) *L*/*R* and (b) *L*/*C* specimen plane showing differences by anatomic location along the length of the femoral diaphysis (percent of total femur length). Differences between values not connected by the same letter for a given anatomic location were statistically significant ($p < 0.05$, Tukey). Asterisks indicate statistically significant differences between anatomic locations for a given model or experimental data ($p < 0.05$, Tukey). Experimental data for the *L*/*R* anatomic plane exhibited differences between each anatomic location, while all other differences between anatomic locations were not statistically significant.

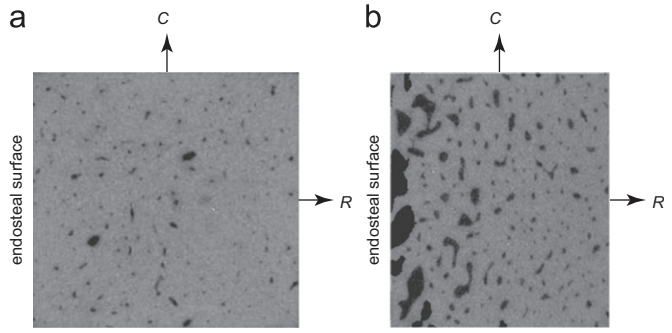


**Fig. 5.** Grayscale micro-CT images of longitudinal specimen cross-sections showing (a) a homogeneous spatial distribution and relatively low volume fraction of intracortical porosity representative of the mid-diaphysis, and (b) a non-uniform spatial distribution and relatively high volume fraction of intracortical porosity near the endosteal surface representative of epiphyseal locations on the femoral diaphysis. The height of each specimen in the *C*-axis is 5 mm.

Kachanov, 2000), but little attention has been given to the effects of the morphology, orientation, and spatial distribution of intracortical porosity.

The greater magnitude and variability of elastic anisotropy in the *L*/*R* plane compared to the *L*/*C* plane (Figs. 2–4), suggests that the primary influence was a non-uniform spatial distribution of intracortical porosity, due to endosteal erosion (Fig. 5). Anatomic variation of elastic anisotropy in the *L*/*R* specimen plane (Fig. 4) was previously reported (Espinoza Orías et al., 2009; Rudy et al., 2011). Endosteal erosion of cortical bone progresses with age (Zebaze et al., 2010) and is more prevalant in the epiphyseal femoral diaphysis. This effect can be readily appreciated by considering that elevated endosteal porosity has relatively little effect on the circumferential elastic constant due to a predominate condition of isostrain (Voigt or upper bound model) (Fig. 5). On the other hand, elevated endosteal porosity has a significant effect on the radial elastic constant due to a predominate condition of isostress (Reuss or lower bound model). Finally, elastic anisotropy in the *L*/*R* specimen plane would also be expected to vary with donor age and gender, but the present study was not designed to investigate this effect. Indeed, a limitation of this study was a small number of subjects ($N=4$).

The combined model accounted for the coupled effects of apatite crystal orientations and intracortical porosity by assigning anisotropic elastic constants derived from the micromechanical model to the finite elements. The combined model provided the most accurate predictions for elastic anisotropy in both the *L*/*R* and *L*/*C* planes (Fig. 2), exhibiting less than 10% mean error (Table 3). Therefore, the combined model may be useful in place of current numerical models, for example, in the study of bone adaptation and metabolic bone disease. Moreover, the approach in this study to couple and decouple the effects of more than one structural feature across more than one length scale using a multiscale, specimen-specific model will be useful to investigate other structure-function relationships in bone tissue. The methods and tools available for multiscale modeling of bone tissue have now advanced to the point where further study should focus on specimen-specific models and data in order to delineate the effects that really matter. Efforts that continue to add to the complexity of models, while comparing predictions to some aggregate of previously published experimental data, have limited ability to gain further understanding of key structure-function relationships.

The combined model predicted tissue orthotropy, but underpredicted the degree of orthotropy (Fig. 2, Table 2) and did not account for anatomic variability of elastic anisotropy in the *L*/*R* plane (Figs. 3 and 4a). This limitation was possibly due to the assumption of constant mineralization levels (apatite crystal volume fraction) in this study. This assumption was based on previous work using a transversely isotropic model which showed little influence of the apatite crystal volume fraction on elastic anisotropy despite being the most significant factor affecting elastic constant magnitudes (Deuerling et al., 2009). The overall mean ( ± standard deviation) tissue mineral density (TMD) for the specimens was 1470 (75) mg HA/cm$^3$, as measured by micro-CT using a custom calibration phantom (Deuerling et al., 2010), supporting this assumption. However, the intra-specimen variability in TMD comprised a Gaussian distribution ranging from just above the intracortical porosity threshold (717 mg HA/cm$^3$) to up to ~2900 mg HA/cm$^3$, with a mean intra-specimen standard deviation of 168 mg HA/cm$^3$. This intra-specimen variability in TMD was not likely uniformly distributed spatially.

Osteonal and newly remodeled tissue adjacent to intracortical porosity exhibits relatively lower levels of mineralization (Meunier and Boivin, 1997) and thus relatively higher strains exacerbated by the presence of stress concentrations (Mullins et al., 2007), compared to interstitial tissue. Therefore, tissue specimens exhibiting a

non-uniform distribution of intracortical porosity concentrated near endosteal surfaces (Fig. 5) would also exhibit relatively lower levels of mineralization near endosteal surfaces (Sansalone et al., 2010). Recall that the more subtle orthotropy ($L/R > L/C$) and variability of elastic anisotropy in the $L/R$ plane was shown to be derived from a non-uniform spatial distribution of intracortical porosity due to anatomic variation in endosteal remodeling. Therefore, the incorporation of voxel-specific mineralization levels in the combined model would be expected to result in the prediction of even greater elastic anisotropy in the $L/R$ plane compared to the $L/C$ plane due to the predominate isostress and isostrain conditions affecting the radial and circumferential elastic constants, respectively, as described above. The incorporation of voxel-specific mineralization levels in finite element models of trabecular bone previously revealed significant effects on tissue-level elastic properties (Jaasma et al., 2002). Therefore, future studies should investigate the incorporation of voxel-specific mineralization levels into the combined model, as well as model sensitivity to the porosity threshold.

Other factors not included in this study are expected to have relatively little effect on the elastic anisotropy of human cortical bone tissue. For example, lacunar–canalicular porosity exhibits directionality at the lamellar level (Schneider et al., 2010) but this directionality in the $R/C$ plane is lost at the tissue level due to homogenization around circular lamellae. Moreover, the volume fraction of lacunar–canalicular porosity is no more than 5% (Cowin, 1999), and was previously shown to exhibit only a minor effect on the elastic properties of cortical bone (Mullins et al., 2007).

## 5. Conclusions

A micromechanical model accounting for the effects of apatite crystal orientations alone accurately predicted the elastic anisotropy of human cortical bone in the $L/C$ plane, but predicted transverse isotropy. A voxel-based finite element model accounting for the effects of intracortical porosity alone significantly underestimated elastic anisotropy in both the $L/R$ and $L/C$ planes, but was able to predict orthotropy. A combined model accounting for both effects provided the most accurate predictions of elastic anisotropy in both the $L/R$ and $L/C$ plane, with less than 10% mean error. Therefore, the results of this study suggest that the dominant and less variable transverse isotropy of human cortical bone, reflected by $L/C$, is governed primarily by apatite crystal orientations, while the more subtle and variable orthotropy, reflected by the difference between $L/R$ and $L/C$, is governed primarily by intracortical porosity.

## Conflicts of interest

The authors have no conflicts of interest to disclose.

## Acknowledgments

This research was partially supported by the U.S. Army Medical Research and Materiel Command (W81XWH-06-1-01960) and the Notre Dame Center for Research Computing.

## References

Akkus, O., 2005. Elastic deformation of mineralized collagen fibrils: An equivalent inclusion based composite model. Journal of Biomechanical Engineering 127, 383–390.

Aoubiza, B., Crolet, J.M., Meunier, A., 1996. On the mechanical characterization of compact bone structure using the homogenization theory. Journal of Biomechanics 29, 1539–1547.

Ashman, R.B., Cowin, S.C., van Buskirk, W.C., Rice, J.C., 1984. A continuous wave technique for the measurement of the elastic properties of cortical bone. Journal of Biomechanics 17, 349–361.

Bousson, V., Meunier, A., Peyrin, F., Bergot, C., Vicaut, E., Rocha, M.A., Morais, M.H., Laval-Jeantet, A.M., Laredo, J.D., 2001. Distribution of intracortical porosity in human midfemoral cortex by age and gender. Journal of Bone and Mineral Research 16, 1308–1317.

Burghardt, A.J., Kazakia, G.J., Ramachandran, S., Link, T.M., Majumdar, S., 2010. Age- and gender-related differences in the geometric properties and biomechanical significance of intracortical porosity in the distal radius and tibia. Journal of Bone and Mineral Research 25, 983–993.

Cooper, D.M.L., Thomas, C.D.L., Clement, J.G., Turinsky, A.L., Sensen, C.W., Hallgrímsson, B., 2007. Age-dependent change in the 3D structure of cortical porosity at the human femoral midshaft. Bone 40, 957–965.

Cowin, S.C., 1999. Bone poroelasticity. Journal of Biomechanics 32, 217–238.

Currey, J.D., 1969. The relationship between the stiffness and the mineral content of bone. Journal of Biomechanics 2, 477–480.

Currey, J.D., Zioupos, P., 2001. The effect of porous microstructure on the anisotropy of bone-like tissue: a counterexample. Journal of Biomechanics 34, 707–708.

Deuerling, J.M., Rudy, D.J., Niebur, G.L., Roeder, R.K., 2010. Improved accuracy of cortical bone mineralization measured by polychromatic microcomputed tomography using a novel high mineral density composite calibration phantom. Medical Physics 37, 5138–5145.

Deuerling, J.M., Vitter, J.S., Converse, G.L., Roeder, R.K., 2012. Micromechanical model for the orthotropic elastic constants of polyetheretherketone composites considering the orientation distribution of the hydroxyapatite whisker reinforcements. Journal of Engineering Materials and Technology 134, 010906 8 pp.

Deuerling, J.M., Yue, W., Espinoza Orías, A.A., Roeder, R.K., 2009. Specimen-specific multi-scale model for the anisotropic elastic constants of human cortical bone. Journal of Biomechanics 42, 2061–2067.

Dong, X.N., Guo, X.E., 2004. The dependence of transversely isotropic elasticity of human femoral cortical bone on porosity. Journal of Biomechanics 37, 1281–1287.

Dong, X.N., Guo, X.E., 2006. Prediction of cortical bone elastic constants by a two-level micromechanical model using a generalized self-consistent method. Journal of Biomechanical Engineering 128, 309–316.

Eppell, S.J., Tong, W., Katz, J.L., Kuhn, L., Glimcher, M.J., 2001. Shape and size of isolated bone mineralites measured using atomic force microscopy. Journal of Orthopaedic Research 19, 1027–1034.

Espinoza Orías, A.A., Deuerling, J.M., Landrigan, M.D., Renaud, J.E., Roeder, R.K., 2009. Anatomic variation in the elastic anisotropy of cortical bone tissue in the human femur. Journal of the Mechanical Behavior of Biomedical Materials 2, 255–263.

Feik, S.A., Thomas, C.D.L., Clement, J.G., 1997. Age-related changes in cortical porosity of the midshaft of the human femur. Journal of Anatomy 191, 407–416.

Fratzl, P., Schreiber, S., Klaushofer, K., 1996. Bone mineralization as studied by small-angle X-ray scattering. Connective Tissue Research 35, 9–16.

Granke, M., Grimal, Q., Saïed, A., Nauleau, P., Peyrin, F., Laugier, P., 2011. Change in porosity is the major determinant of the variation of cortical bone elasticity at the millimeter scale in aged women. Bone 49, 1020–1026.

Halpin, J.C., 1992. Primer on Composite Materials Analysis. Technomic Publishing Co., Lancaster, PA.

Hamed, E., Lee, Y., Jasiuk, I., 2010. Multiscale modeling of elastic properties of cortical bone. Acta Mechanica 213, 131–154.

Hasegawa, K., Turner, C., Burr, D., 1994. Contribution of collagen and mineral to the elastic anisotropy of bone. Calcified Tissue International 55, 381–386.

Hellmich, C., Ulm, F.J., 2002. Are mineralized tissues open crystal foams reinforced by crosslinked collagen?—some energy arguments. Journal of Biomechanics 35, 1199–1212.

Hernandez, C.J., Beaupre, G.S., Keller, T.S., Carter, D.R., 2001. The influence of bone volume fraction and ash fraction on bone strength and modulus. Bone 29, 74–78.

Hogan, H.A., 1992. Micromechanics modeling of Haversian cortical bone properties. Journal of Biomechanics 25, 549–556.

Jaasma, M.J., Bayraktar, H.H., Niebur, G.L., Keaveny, T.M., 2002. Biomechanical effects of intraspecimen variations in tissue modulus for trabecular bone. Journal of Biomechanics 35, 237–246.

Katz, J.L., 1980. Anisotropy of Young's modulus of bone. Nature 283, 106–107.

Katz, J.L., Ukraincik, K., 1971. On the anisotropic elastic properties of hydroxyapatite. Journal of Biomechanics 4, 221–227.

Keller, T.S., Mao, Z., Spengler, D.M., 1990. Young's modulus, bending strength, and tissue physical properties of human compact bone. Journal of Orthopaedic Research 8, 592–603.

Lees, S., Davidson, C.L., 1977. The role of collagen in the elastic properties of calcified tissues. Journal of Biomechanics 10, 473–486.

Meunier, P.J., Boivin, G., 1997. Bone mineral density reflects bone mass but also the degree of mineralization of bone: Therapeutic implications. Bone 21, 373–377.

Mullins, L.P., McGarry, J.P., Bruzzi, M.S., McHugh, P.E., 2007. Micromechanical modeling of cortical bone. Computer Methods in Biomechanics and Biomedical Engineering 10, 159–169.

Niebur, G.L., Feldstein, M.J., Yuen, J.C., Chen, T.J., Keaveny, T.M., 2000. High-resolution finite element models with tissue strength asymmetry accurately predict failure of trabecular bone. Journal of Biomechanics 33, 1575–1583.

Rudy, D.J., Deuerling, J.M., Espinoza Orías, A.A., Roeder, R.K., 2011. Anatomic variation in the elastic inhomogeneity and anisotropy of human femoral cortical bone tissue is consistent across multiple donors. Journal of Biomechanics 44, 1817–1820.

Sansalone, V., Naili, S., Bousson, V., Bergot, C., Peyrin, F., Zarka, J., Laredo, J.D., Haïat, G., 2010. Determination of the heterogeneous anisotropic elastic properties of human femoral bone: from nanoscopic to organ scale. Journal of Biomechanics 43, 1857–1863.

Sasaki, N., Odajima, S., 1996. Stress-strain curve and Young's modulus of a collagen molecule as determined by the X-ray diffraction technique. Journal of Biomechanics 29, 655–658.

Schaffler, M., Burr, D., 1988. Stiffness of compact bone: effects of porosity and density. Journal of Biomechanics 21, 13–16.

Schneider, P., Meier, M., Wedf, R., Müller, R., 2010. Towards quantitative 3D imaging of the osteocyte lacuno-canalicular network. Bone 47, 848–858.

Sevostianov, I., Kachanov, M., 2000. Impact of the porous microstructure on the overall elastic properties of the osteonal cortical bone. Journal of Biomechanics 33, 881–888.

Thomas, C.D.L., Feik, S.A., Clement, J.G., 2005. Regional variation of intracortical porosity in the midshaft of the human femur: age and sex differences. Journal of Anatomy 206, 115–125.

Turner, C.H., Chandran, A., Pidaparti, R.M., 1995. The anisotropy of osteonal bone and its ultrastructural implications. Bone 17, 85–89.

van Rietbergen, B., Odgaard, A., Kabel, J., Huiskes, R., 1996. Direct mechanics assessment of elastic symmetries and properties of trabecular bone architecture. Journal of Biomechanics 29, 1653–1657.

van Rietbergen, B., Majumdar, S., Pistoia, W., Newitt, D.C., Kothari, M., Laib, A., Rüegsegger, P., 1998. Assessment of cancellous bone mechanical properties from micro-FE models based on micro-CT, pQCT and MR images. Technology and Health Care 6, 413–420.

Wagner, H.D., Weiner, S., 1992. On the relationship between the microstructure of bone and its mechanical stiffness. Journal of Biomechanics 25, 1311–1320.

Yue, W., Roeder, R.K., 2006. Micromechanical model for hydroxyapatite whisker reinforced biocomposites. Journal of Materials Research 21, 2136–2145.

Zebaze, R., Ghasem-Zadeh, A., Bohte, A., Iuliano-Burns, S., Mirams, M., Price, R.I., Mackie, E.J., Seeman, E., 2010. Intracortical remodelling and porosity in the distal radius and post-mortem femurs of women: a cross-sectional study. Lancet 375, 1729–1736.

Zioupos, P., Cook, R., Hutchinson, J., 2008. Some basic relationships between density values in cancellous and cortical bone. Journal of Biomechanics 41, 1961–1968.